

Article

Clinopyroxene Crystals in Basic Lavas of the Marsili Volcano Chronicle Early Magmatic Stages in a Back-Arc Transcrustal Mush System

Teresa Trua ¹  and Michael P. Marani ^{2,*} 

¹ Dipartimento di Scienze Chimiche, della Vita e della Sostenibilità Ambientale, Università di Parma, Campus Universitario—Parco Area delle Scienze 157A, 43124 Parma, Italy; teresa.trua@unipr.it

² ISMAR-CNR, Istituto di Scienze Marine, Consiglio Nazionale delle Ricerche, Via Gobetti 101, 40129 Bologna, Italy

* Correspondence: michael.marani@cnr.it

Abstract: Constraining the pre-eruptive processes that modulate the chemical evolution of erupted magmas is a challenge. An opportunity to investigate this issue is offered by the interrogation of the crystals carried in lavas. Here, we employ clinopyroxene crystals from back-arc lavas in order to identify the processes driving basalt to andesite magma evolution within a transcrustal plumbing system. The assembled clinopyroxene archive reveals that mantle melts injected at the crust-mantle transition cool and crystallize, generating a clinopyroxene-dominated mush capped by a melt-rich domain. Magma extracted from this deep storage zone fed the eruption of basalt to basaltic andesite lavas. In addition, chemically evolved melts rapidly rising from this zone briefly stalled at shallow crustal levels, sourcing crystal-poor andesite lavas. Over time, hot ascending primitive magmas intercepted and mixed with shallower cooling magma bodies forming hybrid basic lavas. The blended clinopyroxene cargoes of these lavas provide evidence for the hybridization, which is undetectable from a whole-rock chemical perspective, as mixing involved chemically similar basic magmas. The heterogeneity we found within the clinopyroxene archive is unusual since it provides, for the first time, a complete set of mush-related scenarios by which mantle melts evolve from basalt to andesite compositions. Neither the whole-rock chemistry alone nor the record of the mineral phases crystallizing subsequent to clinopyroxene can provide insights on such early magmatic processes. The obtained clinopyroxene archive can be used as a template for interpretation of the record preserved in the clinopyroxene cargoes of basalt to andesite lavas elsewhere, giving insights into the magma dynamics of the feeding plumbing system that are lost when using whole-rock chemistry.

Keywords: back-arc basin; plumbing system; crystal mush; magma petrogenesis; clinopyroxene



Citation: Trua, T.; Marani, M.P. Clinopyroxene Crystals in Basic Lavas of the Marsili Volcano Chronicle Early Magmatic Stages in a Back-Arc Transcrustal Mush System. *Geosciences* **2021**, *11*, 159. <https://doi.org/10.3390/geosciences11040159>

Academic Editors: Maria Filomena Loreto, Camilla Palmiotto, Paraskevi Nomikou, Manel Prada and Jesus Martinez-Frias

Received: 21 January 2021

Accepted: 29 March 2021

Published: 1 April 2021

Publisher's Note: MDPI stays neutral with regard to jurisdictional claims in published maps and institutional affiliations.



Copyright: © 2021 by the authors. Licensee MDPI, Basel, Switzerland. This article is an open access article distributed under the terms and conditions of the Creative Commons Attribution (CC BY) license (<https://creativecommons.org/licenses/by/4.0/>).

1. Introduction

The definition of the crustal processes by which mantle-derived melts evolve in arc/back-arc volcanoes is important in terms of magma genesis [1–3] and volcanic system architecture [4] and also has implications for continental crust formation [5]. Cooling and crystallization, wall rock assimilation/reaction and magma mixing are the main processes that may modify melts delivered from the mantle during their ascent through the arc/back-arc crust [1,3]. Yet, constraining the mechanisms that govern the chemical evolution of erupted magmas, especially those operating at the early stages of magma differentiation, is not straightforward. Experimental studies reproduce the chemical evolution of co-genetic basic-intermediate arc lavas through closed-system fractionation from hydrous basaltic melts [6–10]. A limitation of these studies, though, is the inability to fully capture the magmatic dynamics that lead to crystals with disequilibrium textures and compositions frequently found in these lava suites [8,11–15]. They provide strong evidence that both closed- and open-system processes govern the chemical evolution of erupted magmas. It

follows that crystal cargoes can help to discriminate between these processes, and thus it is useful to combine mineral information with bulk-rock chemistry in order to fully identify the magmatic history of subvolcanic systems [4,16].

In the present study, we follow this approach to investigate the crustal processing that converted mantle-delivered melts into the spectrum of basalt to andesite lavas erupted at the back-arc setting of the Marsili Volcano (MV), Southern Tyrrhenian Sea (Figure 1a). The whole-rock geochemical (Figure 1b) and isotopic compositions of the MV lavas support a petrogenetic history controlled by fractional crystallization in a melt-rich magmatic environment [17]. However, the plagioclase crystals carried in these lavas [18] preserve evidence that a melt-rich scenario is an oversimplification.

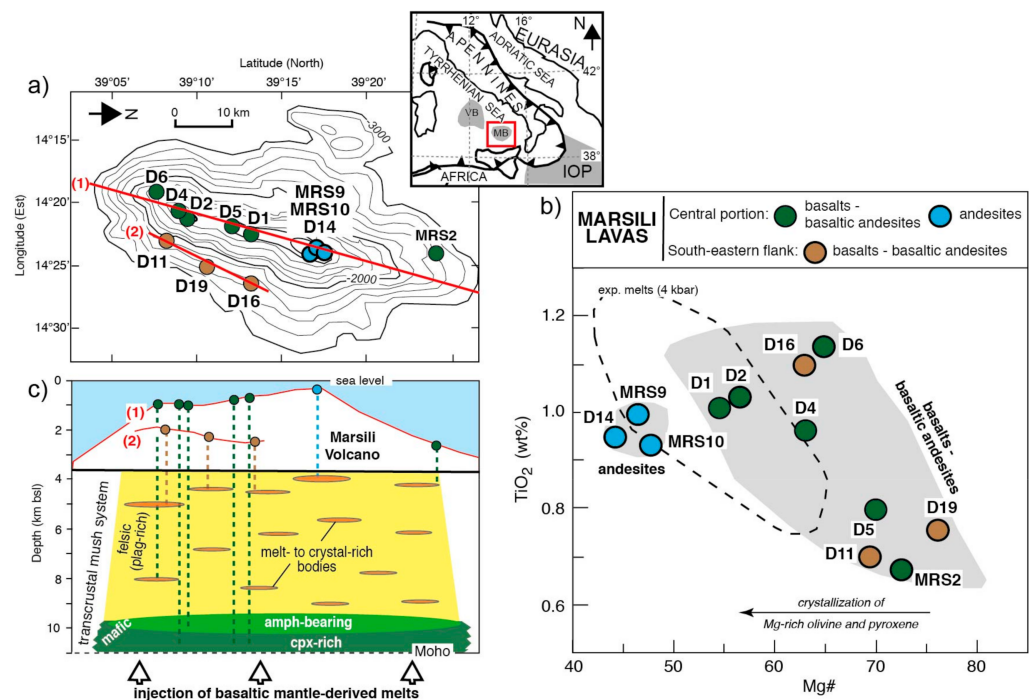


Figure 1. (a) Bathymetry of the Marsili Volcano (MV) back-arc spreading centre (contour interval 200 m)—the location is the red box in the inset. Coloured circles indicate the location of the studied lava samples: the central portion lavas are in green or in light blue in function of the composition; the south-eastern volcano flank lavas are in brown. The numbered red lines represent the tracks of the crustal section shown in (c). The inset shows the locations of the Marsili Basin (MB; red boxed area) and the older Vavilov Basin (VB), the two back-arc basins of the Tyrrhenian Sea. IOP = Ionian Oceanic Plate. (b) TiO₂ content versus Mg# value for the Marsili lavas (grey fields). Lava samples are named and marked with the colour-coded circles of (a): green for basalts and basaltic andesites, light blue for andesites in the central portion, and brown for basalts and basaltic andesites from the south-eastern flank. The black dashed line refers to a field of glasses obtained by low pressure (4 kbar) crystallization experiments simulating chemical evolution of arc-like magmas [8,10]. (c) Cross section of the transcrustal system beneath the Marsili Volcano back-arc spreading centre [18]. For each lava, the crustal storage level, given as depth below sea level (bsf), is based on the results of plagioclase barometric modelling [18] reported in Table 1. Dotted vertical lines, colour-coded as in (a), link storage depth to eruptive sites. The petrological data indicate that the feeding system is compositionally layered: its roots are made of domains transitioning from mafic/ultramafic clinopyroxene (cpx)-rich (dark green) to amphibole (amph)-bearing gabbroic (light green), while the mid to shallow portions contain a network of storage zones (ranging from melt-rich to crystals-rich), set into a felsic, plagioclase (plag)-rich mush.

Table 1. Location, phenocryst assemblage and pre-eruptive conditions of Marsili lava samples discussed in text. All data have been reported in [18]. Phenocryst minerals (i.e., crystals with size > 0.1 mm, with no genetic connection) are listed by order of decreasing abundance (vol%); abbreviations: Ol, olivine; Opx, orthopyroxene; Cpx, clinopyroxene; Pl, plagioclase. Pre-eruptive conditions: set of pressure (P) and temperature (T) conditions [18] at which both plagioclase and pyroxene are liquidus phases. The P (kbar) was used to calculate the pre-eruptive source depth below seafloor (bsf), assuming a density value of $2.9 \times 10^3 \text{ kg/m}^3$, which is equivalent to a lithostatic gradient of 3.5 km/kbar. The source depth below sea level (bsl) was obtained by adding the water depth to the bsf depth.

Rock Type Sample	Location	Phenocrysts	T (°C)	P (kbar)	Pre-Eruptive Conditions		
					Depth (km) below Seafloor (bsf)	Water Depth (km)	Depth (km) below Sealevel (bsl)
Basalts:							
MRS2	northern portion	Ol(12%), Pl(5%), Cpx(2%)	1168–1170	0.3–0.4	1.1–1.4	2.5	3.6–3.9
D5	central rift zone	Cpx(20%), Pl(10%), Ol(2%)	-	-	-	-	-
D6	southern rift zone	Pl(7%), Ol(2%), Cpx(1%)	1143	1.5	5.3	2.6	7.9
D16	south-eastern flank	Pl(8%), Cpx(4%), Ol(2%)	1133–1138	0.5–0.6	1.8–2.1	2.5	4.3–4.6
Basaltic-andesites:							
D1	central rift zone	Pl(8%), Cpx(5%), Ol(1%)	1167–1170	2.5–3.0	8.8–10.5	0.8	9.6–11.3
D2	southern rift zone	Pl(8%), Cpx(2%), Ol(1%)	1142–1148	2.5–3.0	8.8–10.5	0.9	9.7–11.4
D4	southern rift zone	Cpx(8%), Pl(6%), Ol(2%)	1166–1169	2.5–3.1	8.8–10.6	1.0	9.8–11.5
D11	south-eastern flank	Pl(7%), Cpx(3%), Ol(2%)	1139	0.8	2.8	2.3	5.1
D19	south-eastern flank	Pl(10%), Cpx(4%), Ol(2%)	1132–1133	0.4–0.6	1.4–2.1	2.5	3.9–4.6
Andesites:							
MRS9	summit cone	Pl(6%), Cpx(3%)	-	-	-	-	-
MRS10	summit cone	Pl(8%), Cpx(2%), Opx(1%)	-	-	-	-	-
D14	summit cone	Pl(8%), Cpx(2%), Opx(1%)	1141–1145	0.8–1.0	2.8–3.5	0.7	3.5–4.2

In particular, these crystals exhibit anorthite (An) and Mg systematics that suggest the chemical evolution of MV erupted lavas was mainly controlled by crystallization in a mush-dominated regime (Figure 1c), which is undetectable using a whole-rock chemical perspective. Clinopyroxene appears prior to plagioclase at the early differentiation stage of arc magmas due to the hydrous nature of the parent mantle melts [7–10]. The ability of clinopyroxene to address questions related to arc/back-arc magma dynamics is widely demonstrated [11–13,19–21]. Here we focus on the clinopyroxene crystals carried in the lavas previously studied for plagioclase [18] to obtain insights into the magmatic dynamics that are missed by the plagioclase record. We integrate the textural and compositional features of clinopyroxene with thermobarometric information deduced from this and previous petrological studies [18,22] and show how mush-related scenarios, as suggested by theoretical models of transcrustal mush-dominated systems [23], controlled the pre-eruptive history of MV magmas.

2. Background

The MV is a large (c. 70 km × 20 km), NNW-SSE elongated seamount located in the Southern Tyrrhenian Sea (Figure 1a), developed along the spreading centre of the 2 Ma old Marsili back-arc basin [24]. The basin was formed during the last episode of seafloor spreading in the Tyrrhenian Sea, related to the migration of the Alpine suture above the presently north-west subducting Ionian oceanic slab—[25] and references therein. The MV edifice, which was constructed in the last 0.7 Ma, rises 4000 m from the basement level of the basin to a minimum depth of 500 m. Most of the lava samples dredged during several oceanographic cruises are of basalt and basaltic andesite composition; volumetrically minor andesites were sampled at the summit cone of the seamount and likely record the latest stage of volcanic activity (Figure 1b) [24]. The lavas have a back-arc/arc geochemical affinity [17] that is also observed in the Marsili Basin oceanic-type crust [26]. This implies that crustal influence in the genesis of the erupted MV lavas is circumscribed to interactions with co-genetic igneous components. Thus, the minerals crystallized from MV magmas are ideal for investigating the processing that modulates the basalt to andesite chemical evolution of magmas in a back-arc setting.

The comparison of MV lavas with the experimental glasses representing the early evolution stage of arc magmas at pressure conditions < 400 MPa [8,10] (Figure 1b) suggests that most of the differentiation of the MV magmas took place within the local oceanic crust, which extends 10–12 km beneath the Marsili Basin [27]. Furthermore, petrological information [18,22] documents a vertically elongated crustal feeding system, made of stacked and interconnected magma and mush zones (Figure 1c). The system is compositionally stratified, with clinopyroxene- to amphibole-bearing mafic lithologies at the near-Moho horizon, whereas felsic components, with a dominant plagioclase-rich framework, are widespread in the mid to uppermost crustal layers.

3. Materials and Methods

In this study, we examined the texture and composition of a large number (approximately 200) of pyroxene crystals (mainly clinopyroxene with few orthopyroxene) from 12 lava samples (Table 1) fully representative of the MV basalt-to-andesite suite (Figure 1b) and for which petrological information provided by the plagioclase cargo is also available [18]. The phenocryst assemblage of these samples is reported in Table 1 and summarized in Supplementary Materials part 1; detailed petrography is reported in [18]. The whole-rock chemical compositions of the 12 lava samples are reported in Supplementary Materials (Table S1). A large inter-sample range of crystal sizes is observed. In order to fully characterize the petrographic and textural features of the lavas, here we use the term phenocryst to refer to crystals with size > 0.1 mm (measured in the long dimension), with no genetic connotation.

All the basic (basalt and basaltic andesite) lavas are porphyritic, with phenocryst abundance < 20 vol%. In these lavas, the clinopyroxene phenocrysts occur alone and in glomerocryst aggregates, which can be either monomineralic or polymineralic, containing clinopyroxene associated with olivine and plagioclase. The andesite lavas have a lower phenocryst abundance (<11 vol%), comprising small sized plagioclase with scarce clinopyroxene and orthopyroxene. A compilation of thin section photomicrographs is shown in Supplementary Materials (Figures S1–S4).

The analysed pyroxene crystals are representative of the mineral diversity documented under the optical examination of thin sections; see Supplementary Materials part 1. Less spot analyses were obtained for lavas in which the abundance of pyroxene phenocrysts was low. Major and minor element analyses, provided in Supplementary Materials (Tables S2–S12), were performed using a CAMECA S × 50 electron microprobe; see Supplementary Materials part 2. A limited, pre-existing MV pyroxene data set [22], obtained using the same electron microprobe facility, is also included in Supplementary Materials (Table S13).

In order to identify the clinopyroxene compositions acquired at near-equilibrium conditions with the host melt, or re-equilibrated with it, we applied the clinopyroxene-melt thermobarometer models after [28]. These models are considered to be robust [29] and suitable for reconstruction of the P-T conditions of arc magmas [11,12]. We used Equations (30) and (33) of these models [28] for pressure and temperature estimates and considered the bulk-rock composition and loss on ignition (LOI) values (Table S1) as close approximations to melt chemistry and H₂O content, respectively. The standard errors of estimate (SEE) are 170 MPa for pressure and 33 °C for temperature [28]. Each single analysis was tested for equilibrium with the respective host melt by applying the two filters recommended by [28], as explained in Supplementary Materials part 3 and illustrated in Figure S5. Data points that passed both the equilibrium filters are shown in Supplementary Tables S2–S13 and are reported as PX-08 in the text.

As an independent test for the validity of the clinopyroxene-melt thermobarometric approach, we ensured that the PX-08 estimates were consistent with those obtained by the MELTS algorithm [30], used to determine the plagioclase crystallization conditions on the same lava samples [18]. This comparison is possible since clinopyroxene is included in the equilibrium mineral assemblage returned by MELTS simulations, hereafter referred to as

PX-MELTS. The PX-08 (this study) and PX-MELTS [18] calculations define instantaneous crystallization conditions that obey equilibrium phase relations. Hereafter, we use the Mg# value ($Mg\# = Mg / (Mg + Fe_{tot})$) of the equilibrium clinopyroxene composition yielded by these calculations to define the Mg# equilibrium window linked to these specific conditions in the carrier magma. Likewise, the clinopyroxene compositions with Mg# plotting outside this window, at more evolved (lower Mg#) and/or more primitive (higher Mg#) compositions, provide evidence for deviations from equilibrium conditions and can be used to investigate magma open system evolution over the period of crystal growth.

The calculated pressures (kbar) were converted to depth below sea floor (Km bsf), assuming crustal density of 2900 kg/m^3 [18] for the oceanic crust below the MV. Among the dredged sites, the water depth is highly variable (ranging from 0.7 to 3.0 km; Figure 1a), and therefore, for each lava sample, we calculated the pre-eruptive source depth below sea level (km bsf) by adding the water depth to the modelled depth bsf (Table 1).

4. Results

4.1. Chemical Variability of MV Clinopyroxene

MV pyroxene crystals range from diopside to augite clinopyroxene; few crystals classify as enstatite orthopyroxene; see Supplementary Materials (Figure S6). An inspection of the analysed clinopyroxene cargoes (Tables S2–S13) reveals intra- and inter-crystal chemical variability, such as significant variation in Mg#, that exceeds the respective equilibrium window for Mg# in clinopyroxene, coupled with a large variation in other chemical elements (Figures 2–4; Figure S7 in Supplementary Materials).

In igneous clinopyroxenes, Mg-Fe interdiffusion typically occurs on a much faster time scale than the diffusion of other elements [31,32]. The chemical variability of MV clinopyroxene cargoes implies that the timescale of crystal residence within the carrier magma prior to eruption was short enough to prevent deletion of the chemical gradients by diffusivity.

In the following sections, we describe the variation observed in the clinopyroxene major and minor element content (wt%) versus the Mg# value in conjunction with petrographic observations. Evidence is found for two subgroups of clinopyroxene cargoes: one recording melt evolution by crystallization stages in a mush setting and the other representing the products of magma mixing associated with the injection of primitive magma into pre-existing storage zones.

4.1.1. Crystallization in the Mush

The most primitive clinopyroxene cargoes (Mg# from 0.92 to 0.75) in basalt and basaltic andesite lavas display trends in chemical element concentrations versus Mg# that furnish details about fractionation in primitive basaltic mantle melts. Ti, Na and Al are incompatible elements in clinopyroxene formed in a cooling basaltic melt [33], but we only observe a clear linear trend for the Ti content, which increases with decreasing Mg# (Figure 2a). Instead, Na- and Al-Mg# trends are scattered, with a large variation in element concentration at a fixed Mg# (Figure S7), suggesting that the behaviour of these elements is also influenced by growth kinetics [29] and, at least for Na, is pressure dependent [28]. The linear Ti-Mg# trend, shown by the primitive clinopyroxene cargoes in three basic lavas (i.e., the D5 basalt, and the D1 and D4 basaltic andesites), records the early stage (Stage A) of MV magma evolution. Indeed, this trend mirrors the one predicted for the early differentiation of hydrous basaltic melts by olivine + clinopyroxene fractionation in a closed system [10,34]. Crystals growing in this system are, however, expected to exhibit normal zoning, documented by Mg# decrease from core to rim while TiO_2 increases. Instead, most of the primitive crystals carried in each of these basic lavas show complex zoning, encompassing, with their core to rim chemistry, a large segment of the TiO_2 -Mg# trend (Figure 2a). This observation implies chemical variability in the melt surrounding the crystals at the time of their growth, compatible with the chemical gradient expected for the melt fraction across a mush environment. Similar TiO_2 -Mg# patterns are indeed

observed in high-Mg# clinopyroxene crystals from exhumed island arc crustal sections [35] and erupted lavas [36,37], representing crystallization in deep crustal mush environments (Figure 2a).

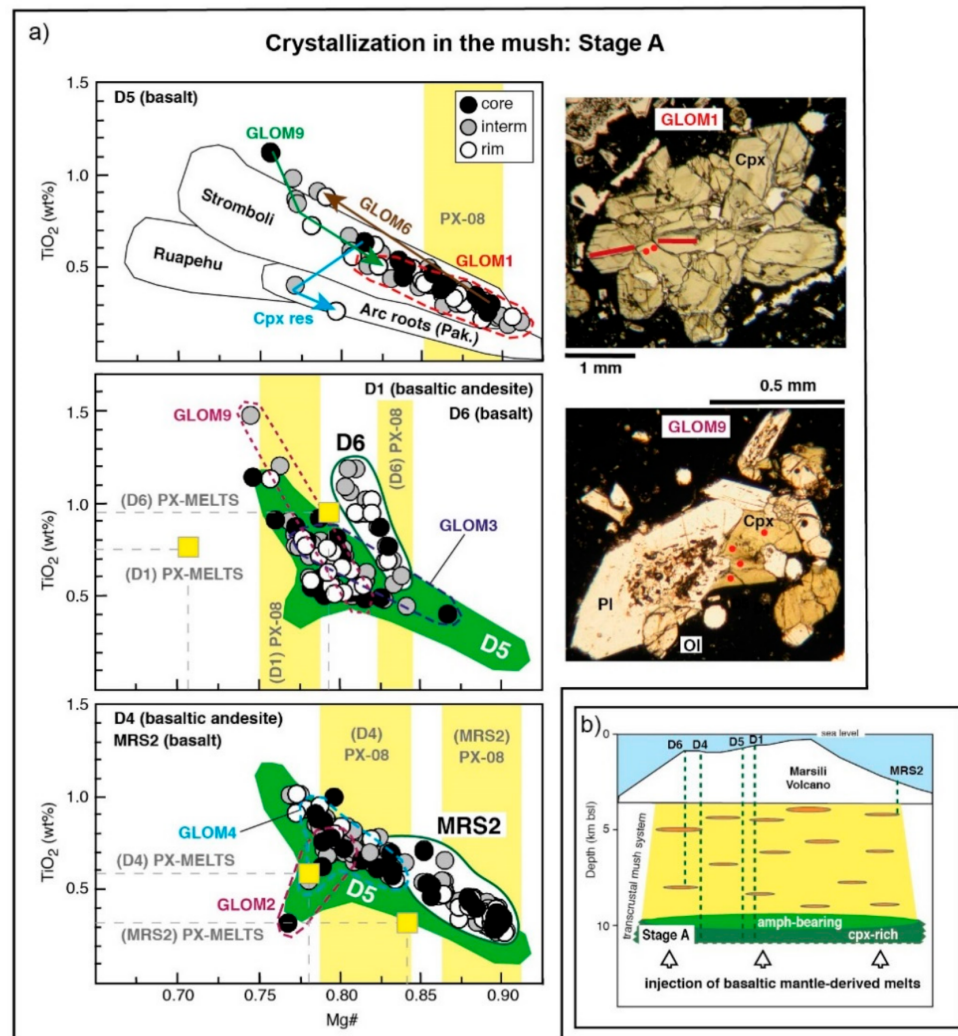


Figure 2. Clinopyroxene variability indicative of Stage A crystallization. (a) TiO_2 (wt%) versus $\text{Mg}\#$ for the clinopyroxene crystals in basalts to basaltic andesite lavas, top to bottom: D5; D1 and D6; MRS2 and D4. Estimated analytical error (2 standard deviation) was smaller than symbol size. The yellow box and the yellow vertical band refer to the $\text{Mg}\#$ equilibrium values indicated by the PX-MELTS [18] and the PX-08 (this study) results, respectively. Analyses of selected crystals (single or in glomerocrysts) are indicated with their abbreviation (see Supplementary Tables S2–S13) and marked with coloured arrows connecting core to rim or enclosed within dashed lines. The D5 clinopyroxene field is reported in green. Photomicrographs under parallel nicols are reported for some crystals (location of the analysed transects or points marked by red lines or dots, respectively); further photomicrographs are reported in Supporting Materials (Figure S1). Mineral abbreviations: Ol = olivine; Cpx = clinopyroxene; Pl = plagioclase; Glomerocrysts = GLOM. The $\text{Mg}\#$ - TiO_2 trend exhibited by these cargoes identifies “Stage A” cooling and crystallization during melt percolation at the pre-eruptive storage zone at the base of the MV crust, outlined in (b). Black lines enclose clinopyroxene compositions found at island-arc settings, recording growth in deep crustal mush environments: basic lavas from Stromboli [37] and Ruapehu [36]; exhumed island arc crustal section [35]. (b) Cross section of the multitiered magma plumbing system beneath Marsili Volcano, as in Figure 1c. Box “Stage A” marks location of deep crystallization events recorded by the D5, D4 and D1 clinopyroxene cargoes.

Cr is highly compatible in high Mg# clinopyroxene formed at the early differentiation stages of basaltic magma [38], and the decrease of the Cr₂O₃ content (from 1.1 wt% to complete depletion) observed at the 0.80–0.90 Mg# range (Figure S7) is consistent with this scenario. However, we do not observe a rapid Cr decrease with decreasing Mg#, as expected for crystals recording growth in a single cooling basaltic melt. Instead, we find a scattered Cr distribution, likely due to the injection of mantle-derived melts into the environment in which the primitive clinopyroxene crystals were growing. This process is invoked to explain this type of Cr-Mg# distribution in primitive clinopyroxene elsewhere [36,38,39]. Furthermore, we observe that Cr variation in MV primitive clinopyroxene crystals is not positively correlated with Al, an element that, like Cr, has a slow diffusion in clinopyroxene [39], excluding that the behaviour of Cr was controlled by growth kinetics. Finally, the linear inverse FeO_{tot}-Mg# trend exhibited by these crystals indicates that FeO variations have no effects on the element systematics discussed above (Figure S7).

The crystal systematics of the few clinopyroxene crystals carried in two basalts (MRS2 and D6) are also reported in Figure 2a. These crystals exhibit a primitive signature (Mg# ranging from 0.80–0.90) consistent with near-equilibrium growth in the respective carrier magma. In particular, the MRS2 clinopyroxenes are compositionally similar to the most primitive found in the D5 basalt. Instead, the D6 clinopyroxenes exhibit a marked chemical gradient within a narrow Mg# range (Figure 2a) indicative of rapid crystal growth [22].

Among the MV basic lavas, the clinopyroxene crystals carried in the D2 basaltic andesite show the widest chemical variability, with a similar correlation of TiO₂ and Al₂O₃ with Mg# (Figure 3a and Figure S7). In detail, the D2 clinopyroxene field overlaps with the most evolved compositions of the D5 clinopyroxene, before splitting into two branches recording lower and higher TiO₂ and Al₂O₃ concentrations with decreasing Mg#. The branches overlap at the Mg# equilibrium window of the D2 lava and point towards the compositional fields of the few orthopyroxene (this study) and amphibole [22] crystals found in this lava (Figure 3a). Some crystals are mantled by a thin (10 microns) clinopyroxene rim (Supplementary Materials part 1) with the lowest Mg# values of the D2 cargo, coupled with a large variation in the content of Ti (Figure 3a) and the other analysed elements (Figure S7). The finding of mantled orthopyroxenes and amphibole crystals indicate reaction with the carrier magma, implying an antecryst origin.

It is evident that the Ti-Mg# and Al-Mg# trends exhibited by D2 clinopyroxene cargo (Figure 3a and Figure S7) and the forked shape at the lower Mg# values documented a gradual transition from Stage A to a new stage (Stage B) in magmas evolving from parental basaltic melts by gabbroic fractionation, which led to conditions approaching orthopyroxene + amphibole crystallization but not attaining them. Clinopyroxene crystals exhibiting the D2-like Ti-Al-Mg# fingerprint are reported in other basic arc igneous rocks (Figure 3a), generated by a crystallization history that also involved amphibole fractionation [32,40,41]. Depletion in TiO₂ with decreasing Mg# value in the D2 clinopyroxene cargo could also indicate that Fe-Ti oxides saturation conditions were reached at the melt-rich storage zone, too (Figure 3c).

Andesite lavas (i.e., MRS9, MRS10, D14) are characterized by a low content (<11%) of small-size (<0.2 mm) phenocrysts dominated by plagioclase and accompanied by clinopyroxene and opaque (Table 1). Thus, a low number of clinopyroxene crystals were measured in the andesite lavas. These crystals show a restricted Mg# range (from 0.72–0.77), which plots close to the Mg# equilibrium value obtained by the MELTS calculations (Figure 3b). None of the clinopyroxene analyses passed the PX-08 equilibrium test (Figure S5). However, the narrow Mg# range is coupled with a large variation in the concentration of Ti (Figure 3a) and the other elements (Figure S7), except for Cr, which exhibits very low content as expected for evolved clinopyroxene compositions. Overall, the andesite clinopyroxene compositions display a close match with the most differentiated end of the D2 clinopyroxene field (Figure 3b), suggesting that the andesite lavas were produced by a further fractionation stage (Stage C) from a parental D2 basaltic andesite melt. Clinopyroxene

crystallization was evidently not important at this fractionation stage, as in such a case, a shift to lower Mg# values should be observed in the andesite (Figure 3b). Indeed, the Ba-Sr systematics of the bulk MV plagioclase [22] indicate a basaltic andesite to andesite chemical evolution driven by crystallization dominated by plagioclase, consistent with the andesite phenocryst assemblage (Table 1).

4.1.2. Magma Mixing Processes

Distinctive clinopyroxene features found in some basic lavas document that mixing of magmas took place during magma storage and crystallization. This is the case of the D16 basalt, and the D11 and D19 basaltic andesite lavas erupted at the off-axis, MV south-eastern flank (Figure 1).

In each of these lavas, the clinopyroxene cargo displays a similar range (0.70–0.90) in the Mg# value, irrespective of the chemistry of the carrier lava (Figure 1b), coupled with a high chemical variability (Figure 4 and Figure S7). Focusing on the TiO₂-Mg# distribution (Figure 4), we observe the following: the equilibrium Mg# window is at the high-Mg# end of the respective clinopyroxene range for each of these lavas; most of the primitive (Mg# > 0.80) compositions exhibit linear TiO₂-Mg# trends, consistent with the crystallization conditions recorded by the D5 clinopyroxene cargo; the more evolved compositions (Mg# = 0.70–0.75) are found in small antecrysts with cores of clinopyroxene or orthopyroxene, closely resembling compositions found in the D2 basaltic andesite.

The highly heterogeneous clinopyroxene population of these three lavas exhibit most of the variety of textural and compositional features of the previously described clinopyroxene cargos.

In addition, only these lavas carry partially resorbed clinopyroxene crystals and gabbroic clots with open, sub-circular textures (see Supplementary Materials part 1). The former feature is indicative of crystals that underwent thermal disequilibrium, whereas the latter record growth in a melt-rich magma. In some cases, the compositions of both resorbed crystals and clinopyroxene in the gabbroic clots fall within the Mg# equilibrium window (Figure 4), implying formation from compositionally similar (in terms of major elements) basic magmas. Overall, these textural and compositional features represent strong evidence for blended clinopyroxene populations formed by mixing events involving basic magmas, each with its own crystal cargo.

4.2. Pressures and Temperatures of Crystallization

The pressure-temperature (P-T) paths followed by the MV lavas were investigated by using the PX-08 clinopyroxene-melt thermobarometric model [28] and comparing the obtained estimates with previously identified magma storage conditions [18,22].

A low number of clinopyroxene analyses in the basic lavas and no analyses in the andesite lavas passed the recommended PX-08 equilibrium tests (Figure S5). The estimates referred to the clinopyroxene-melt pairs that passed the tests define the subvertical P-T paths, mostly parallel to each other (Figure 5) and indicative of crystallization across a pressure interval of 0–4 kbar spanning the MV crust thickness (Figure 1c). The PX-08 results agree with the PX-MELTS calculations [18], covering much of the P-T space identified by PX-MELTS data and extending to higher pressures (Figure 5). However, the PX-08 barometric estimates display a large spread in the pressure values for each of the lava samples and are thus not able to indicate the most likely among the pre-eruptive storage conditions, which are instead identified by the MELTS simulations (Figure 1c). This is to be expected due to the large uncertainty (170 MPa) in the crystallization pressures, estimated by the PX-08 barometric model, which becomes larger in shallow conditions (<3 kbar) [42] akin to those expected across the MV crust (Figure 1c).

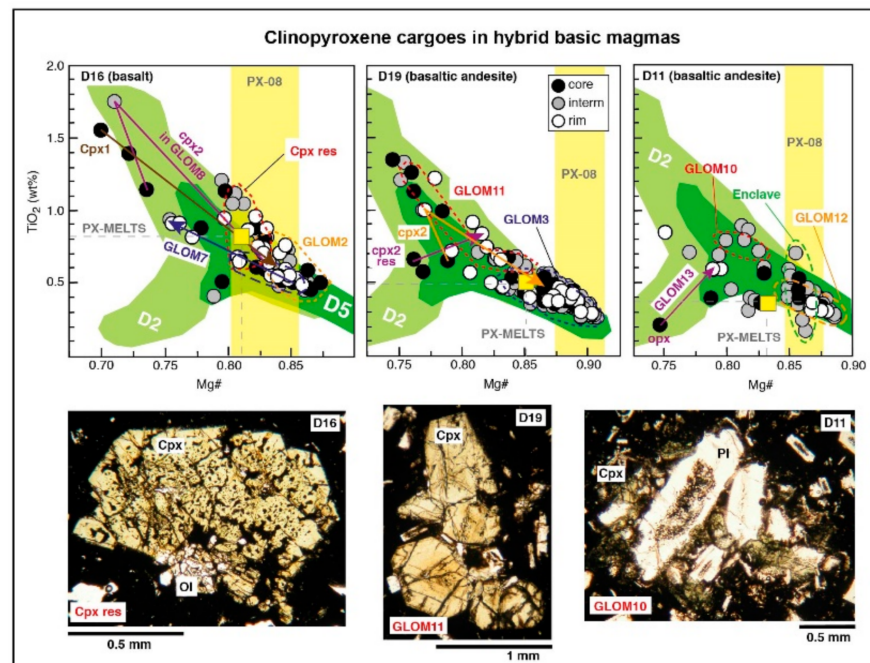


Figure 4. Plots of TiO₂ (wt%) versus Mg# for the clinopyroxene cargoes in the D16 basalt, and D11 and D19 basaltic andesites. These are hybrid basic lavas erupted at the MV south-eastern flank (Figure 1a). Note that these cargoes display a similar chemical variability, irrespective of the chemistry of the carrier lava, that covers most of the D5 and D2 fields. The crystals are tagged as in Figure 2; further photomicrographs are reported in Supporting Materials (Figures S3 and S4). Only in these lavas, partially resorbed clinopyroxene crystals (Cpx res) and gabbroic clots with open, sub-circular texture (Enclave) were found. Analytical error, yellow box and vertical band are displayed as in Figure 2. Light and dark green fields represent D2 and D5 clinopyroxenes, respectively, recording Stage A and Stage B crystallization in the deep MV mush.

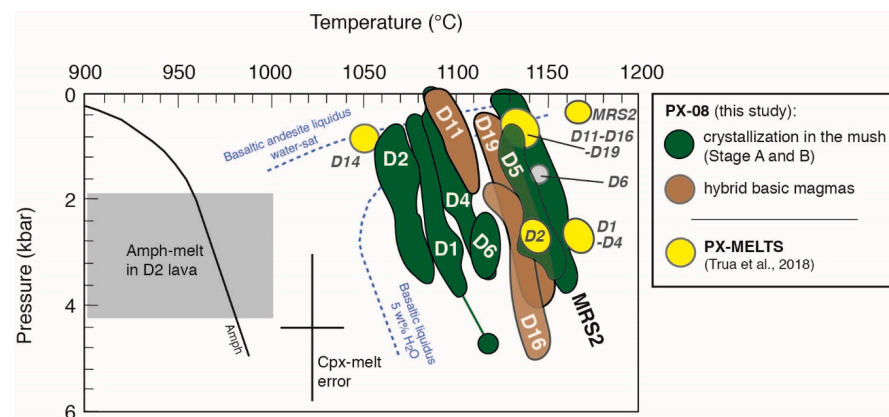


Figure 5. Results of the PX-08 calculations. The coloured fields represent the sets of calculated pressure-temperature for clinopyroxene-melt pairs in the studied lavas that passed the PX-08 tests (see Figure S5 in Supplementary Materials); the colour-code is the same as in Figure 1. For comparison, the PX-MELTS-derived values (yellow circles) are shown [18]. The clinopyroxene-melt pairs in basalts and basaltic andesites from the MV central portion (green fields) illustrate the P-T conditions for Stage A and Stage B crystallization in the mush; those in basalts and basaltic andesites from the south-eastern flank of the MV (brown fields) illustrate the P-T conditions for hybrid basic magmas. The P-T field obtained from D2 amphibole thermobarometric calculations [22] is also reported in the grey box. The liquidus (liquid to the right of each line) for basalt with 5 wt% H₂O and water-saturated basaltic andesite (blue dotted lines) and the amphibole-in boundary line in black (amphibole to the left of the line) are from [43].

We evaluated the effect of melt H₂O concentration on the calculated PX-08 temperature and pressure estimates by also performing PX-08 calculations at ± 1 wt% of the whole rock LOI content (whole-rock LOI ranges from 0.7–2.2 wt%; Table S1). Temperature and pressure estimates resulting from these calculations reflect variations of about 15 °C/wt% and 20 MPa/wt%, which are within the PX-08 geothermometer uncertainty [28].

With reference to temperature, the PX-08 calculations yielded a range of 1060–1160 °C, with the highest and the lowest values referred to the nominal melts of the MRS2 basalt and the D2 basaltic andesite, respectively (Figure 5). However, there is no indication of a progressive decrease in temperature as the host melt evolves from basalt to basaltic andesite compositions, suggesting that not all the MV basic lavas were produced by fractional-crystallization processes alone.

As reported in [22], the amphibole-bearing lithologies carried in the D2 lava provide a record for cooling and crystallization of hydrated basic magmas within the MV plumbing system, at depths corresponding to 2–4 kbar of pressure (Figure 5). The PX-08 results indicate that the ascending D2 magma was less hydrated than a basaltic melt with 5 wt% of H₂O [43] and must have had a high temperature when crossing the amphibole-bearing magma storage region. These results support the view that amphibole-bearing lithologies were captured by the D2 magma when it traversed the MV amphibole-bearing crust.

5. Discussion

Our data show that the Mg#-TiO₂ systematics in clinopyroxene better record the effects of the processes that sourced the erupted MV magmas. Similarly, the study of the MV plagioclase demonstrated that An-Mg variations exhibited by these crystals (Table S14) supply further details of MV crystallization history [18]. In this section, we combine the information supplied by the clinopyroxene textural features and the Mg#-TiO₂ systematics with the information supplied by the plagioclase study [18]. Using this approach, we reconstruct the spectrum of magma storage and transport processes operating at crustal levels of the < 0.7 Ma MV plumbing system that led to eruption of basalt to andesite lavas.

5.1. Crystallization Stages Governing Basalt-Andesite Evolution

Barometric results obtained in this study and in previous work [18,22] yielded the deepest pre-eruptive storage conditions for the D1, D4 and D5 basic lavas (Figure 1). The clinopyroxene cargo in these lavas provides information on the early stage of crystallization (Stage A) of the MV magmas. Indeed, the linear TiO₂-Mg# trend defined by these primitive clinopyroxene cargoes (Figure 2a) is consistent with crystal growth in a cooling mush environment, formed when hydrous basaltic mantle-derived melts entered and stalled at the base of the MV back-arc crust (Figure 2b). The Cr-Mg# systematics (Figure S7) indicate that this stage was influenced by a continuous injection of primitive melts, a necessary mechanism for the formation of a deep crustal mush body according to theoretical models [23].

Most of these primitive clinopyroxene crystals are found in glomerocrysts that vary from locked clinopyroxene clusters to polymineralic aggregates (Figure 2b and Supplementary Materials part 1). Polymineralic aggregates are made of slightly more differentiated clinopyroxene (Mg# < 0.85) associated to Mg-rich olivine (Fo < 80) and An-rich (An₈₀₋₉₀) plagioclase. These clinopyroxene-bearing glomerocrysts are likely fragments of the deep mafic/ultramafic to gabbroic mush region, formed at Stage A (Figure 2b). Indeed, the variability observed in the fabric and mineralogy of these glomerocrysts documents a progressive crystallization process controlled by clinopyroxene segregation, with a minor role for olivine and with plagioclase joining the crystallization sequence later. This sequence is the same found in the exposed roots of volcanic arcs [35] and in crystallization experiments on arc melt compositions [8,10]. It documents the early stage of differentiation in hydrous arc magmas.

Among these deep-sourced clinopyroxene cargoes, only the glomerocrysts carried in the D4 basalt exhibit a narrow Mg# range that overlaps the equilibrium window (Figure 2a),

suggesting that the carried glomerocrysts were collected from the mush portion feeding the erupted lava (Figure 2b). Instead, the clinopyroxene cargoes in the D5 and D1 lavas exhibit a Mg# range wider than the respective equilibrium windows (Figure 2a), extending to more evolved and more primitive compositions, respectively. We suggest that the heterogeneity in the clinopyroxene compositions found in the D5 and D1 lavas supply a view of the entire clinopyroxene chemical variability in the Stage A mush storage zone (Figure 2b). Eruption conditions were probably more vigorous for the D5 magma than for the D1 and D4 magmas, facilitating the entrainment of more primitive clinopyroxene crystals from the lower part of the mush. Furthermore, the high abundance (20 vol%) of clinopyroxene in the D5 basalt (Table 1) implies that the carrier magma maintained enough ascent velocity to avoid settling during transport of the clinopyroxene cargo, thus precluding any long-term storage during magma rise from the deep mush storage zone to the surface.

Both the thermobarometric PX-08 estimates and the PX-MELTS calculations agree that the D2 basaltic andesite lava was also sourced from the deep MV crust (Figure 5). The pyroxene cargo carried in this lava exhibits a wide variation in terms of Mg# versus chemical elements, defining a field that mostly overlaps the D5 clinopyroxene field, representative of Stage A conditions, and extending to more evolved pyroxene compositions (Figure 3a). The D2 pyroxene cargo thus documents a subsequent stage in the formation of the MV deep-crustal mush environment (Stage B). According to theoretical models, as compaction proceeds within the deep crystal mush, residual melts are expelled upward and may accumulate in an overlying melt-rich region, where cooling and crystallization shift the melt toward more silica-rich compositions [23]. Convection is expected to be induced in this melt-rich region, leading to thermo-chemical fluctuations by overturn and stirring, generating a diversity of mineral textures and compositions [44,45]. The heterogeneity in the textural and compositional features found in both the pyroxene (this study) and plagioclase [18] cargoes of the D2 basaltic andesite lava is in line with an origin of the feeding magma from this type of environment. We thus suggest that the D2 magma was extracted from a melt-rich region capping the clinopyroxene-bearing mush domain formed at the roots of the MV feeding system (Figure 3c). Amphibole and orthopyroxene antecrysts are found in D2 lava as single crystals or in glomerocrysts coupled to An-rich plagioclase [22]. These antecrysts provide evidence that D2 magma migrated through a pre-existing amphibole-orthopyroxene basic lithology, formed at 7–14 km depth (Figure 1) by the cooling of melts geochemically similar to D2 but more water-rich [22]. Some of these antecrysts were mantled by thin clinopyroxene rims that document, with their chemical variation (Figure 3a), the D2 melt heterogeneity present during rim growth and the entrainment of the antecrysts shortly before eruption.

In the crystal-poor andesite lavas, none of the clinopyroxene analyses passed the PX-08 tests (Figure S5). The results of the MELTS modelling [18] indicate shallow storage zones for these lavas, located at the base of the MV edifice (0.8–1.0 kbar; Figure 1). MELTS simulations also yielded orthopyroxene and plagioclase as liquidus phases, with compositions resembling those found in the orthopyroxene (Figure 3b) and plagioclase crystals [18] carried in the andesite lavas, while clinopyroxene results absent. Instead, we found clinopyroxene crystals in andesite lavas, and these crystals exhibit chemical systematics resembling those of the more evolved pyroxene compositions extracted from the Stage B storage zone (Figure 3b). This finding documents a subsequent stage (Stage C) in the formation of the MV crustal mush environment. We suggest that the andesitic melts extracted from the Stage B storage zone were able to travel along an adiabat, intersecting orthopyroxene and plagioclase liquidus at the shallower storage zone [46], as indicated by MELTS results. Clinopyroxene crystallized later during Stage C (Figure 3c), as also indicated by the finding of clinopyroxene sub-ophitic arrangement with the plagioclase crystals in the andesite lavas (Figure 3b). Continued cooling at the Stage C level formed plagioclase-rich mush bodies due to the plagioclase-dominated crystallization at this shallow storage region (Figure 3c). As discussed in the previous plagioclase study [18], the compacted glomerocrysts, carried by MV lavas and made almost entirely of An-poor plagioclase crystals (Table S14), are

the final cooling products at the Stage C level and represent fragments of the felsic mush widespread at the shallower portion of the MV transcrustal system (Figure 1).

5.2. Basic Magma Migration Pathways

Considered together, the clinopyroxene (this study) and the plagioclase [18] records from the MV basic lavas give valuable indications of the migration modes followed by feeding magmas within the MV transcrustal system (Figure 1).

Among the deep-sourced basic lavas, D1, D4 and D5 lavas carry dense, high Mg# clinopyroxene crystals (Figure 2a), implying that the feeding magmas must have risen rapidly to the surface from the inferred pre-eruptive storage zone (Stage A, Figure 2b), preventing settling of their clinopyroxene cargo. This scenario is also in line with the plagioclase cargo of these lavas that share a narrow, An-rich compositional range, coupled with An-Mg variations (Table S14) that document feeding magmas delivered to the surface without further significant crystallization. This does not hold for the D2 lava, which carries clinopyroxene crystals with a large texture and compositional heterogeneity, resulting from a magma sourced from the deep mush region (Stage B, Figure 3c) and subsequently migrating through a vertically extended melt-rich mush column [18]. Indeed, the heterogeneity observed in the An-Mg systematics of the D2 plagioclase cargo (Table S14) can only result from the crystallization of magma traversing this pathway.

The D6 and MRS2 basic lavas, sourced from mid-shallow storage levels (Figure 1c), carry few clinopyroxene crystals with high Mg# values (0.80–0.90) close to the equilibrium conditions (Figure 2a). The clinopyroxene data obtained for these two lavas are too scarce to supply valid indications about magma migration pathways, but this information can be acquired from their plagioclase cargoes [18]. Indeed, the MRS2 plagioclases exhibit a marked Mg gradient at a narrow, An-rich composition (Table S14) that likely results from the fast transport of the host melt in conduits or dykes. Instead, the D6 plagioclases exhibit a heterogeneity in the An-Mg systematics that resembles the one observed in the D2 plagioclase cargo (Table S14), indicating that the feeding magma passed through a mush section that was melt-rich at the time of lava eruption.

The D16 basaltic and the D11 and D19 basaltic andesite lavas—erupted at the off-axis, southeastern flank of the MV (Figure 1)—carry clinopyroxene cargo showing texture and compositional evidence for a pre-eruptive open-system scenario. Indeed, the heterogeneity found in the clinopyroxene cargo of these basic lavas clearly documents a hybrid nature, linked to the intrusion of a hot basic magma into a colder, basic magma storage zone that PX-08 and MELT-08 barometric results locate at 4–5 km bsl (Figures 1 and 5). Furthermore, in each of these lavas, the heterogeneity in the features of the clinopyroxene crystals spans much of the variety observed for Stage A and Stage B clinopyroxenes (Figure 4), indicating that some of these crystals were collected from the deep MV mush crust. Further textural evidence is the primitive, partially resorbed clinopyroxene crystals (Figure 4), likely formed due to the entrainment of crystals into a higher-temperature basic magma [47], and the gabbroic crystal clots with open sub-circular texture (Supplementary Materials part 1), both probably representing fragments of the intercepted cooling magma/mush storage zones. The fact that the clinopyroxene cargoes in all the three lava samples display a similar broad range in Mg# value, with the respective equilibrium clinopyroxene crystallization window lying at the high Mg# end of this field (Figure 4), argues in favour of a mixing scenario between basic magmas close in compositions in terms of major elements. This setting would explain why the PX-08 model yielded similar temperature estimates for the transient equilibrium clinopyroxene crystallization of these lavas, despite the bulk-rock chemistry varies from basalt to basaltic andesite (Figure 1). It is also in line with the narrow, An-rich compositional range of the plagioclase cargo of these lavas (Table S14), the An-Mg signature of which indicates that the feeding basic magmas experienced limited crustal interaction upon ascent to the surface [18].

6. Conclusions

Through the study of the clinopyroxene cargoes carried in basalt to andesite lavas, we furnish details of the stages of magma evolution as it migrates through the 10–12 km thick transcrustal mush system of a young, oceanic back-arc spreading centre. We found clinopyroxene populations with chemical and textural features indicative of differentiation in the deep crust. Here, repeatedly injected hydrous mantle-derived melt created, in time, favourable conditions for the formation of a mafic-ultramafic mush zone from which basalt and basaltic andesite magmas were sourced. Clinopyroxene in the phenocryst-poor andesite lavas instead record shallower growth, likely occurring in evolved melts extracted from the deep mush region and stalled at the base of the volcano. Furthermore, examination of the detailed clinopyroxene archive enabled the recognition of hybridization among the erupted basic magmas, produced by the interception and mixing of upward migrating crystal-bearing magma with pre-existing, mid-crustal magma/mush bodies. The hybrid products contribute to the overall volume of the erupted basic lavas, but they may go undetected using a traditional chemical approach, since the involved magmatic components have a common basic bulk rock composition. The blended nature of these lavas is missed in the mineral phases growing subsequent to clinopyroxene in the respective magmas.

Combining information provided by the clinopyroxene composition with the information available on the plagioclase cargoes of the lavas, we identify the complexity of the pre-eruptive conditions within the transcrustal mush region traversed by the carrier magma. Distinctive insights are also acquired into the physical state (more or less crystal-rich) of the mush zones in the plumbing system.

A comparison of the MV clinopyroxene assemblage with the clinopyroxene records from a number of basaltic to andesitic arc/back-arc magmas indicates that the mush-related scenarios identified here could be widespread in these settings. Since the obtained archive provides a record of magma history covering the entire local transcrustal mush column, it can be used as a template to interpret the clinopyroxene populations found elsewhere. This would help to identify the still underappreciated mush-related scenarios in magma evolution history.

Supplementary Materials: The following are available online at <https://www.mdpi.com/article/10.3390/geosciences11040159/s1>, Figure S1: Textural features of pyroxene crystals from D5 basalt, Figure S2: Textural features of pyroxene crystals from D2 basaltic andesite, Figure S3: Textural features of pyroxene crystals from D11 basaltic andesite, Figure S4: Textural features of pyroxene crystals from D16 basalt, Figure S5: Clinopyroxene-melt equilibrium tests, Figure S6: Pyroxene quadrilateral classification diagram, Figure S7: Pyroxene crystals compositional variation, Table S1: Location, phenocryst assemblage, whole-rock analyses and pre-eruptive conditions of Marsili lava samples, Table S2: pyroxene analyses of sample MRS2, Table S3: pyroxene analyses of sample D5, Table S4: pyroxene analyses of sample D16, Table S5: pyroxene analyses of sample D1, Table S6: pyroxene analyses of sample D2, Table S7: pyroxene analyses of sample D4, Table S8: pyroxene analyses of sample D11, Table S9: pyroxene analyses of sample D19, Table S10: pyroxene analyses of sample MRS9, Table S11: pyroxene analyses of sample MRS10, Table S12: pyroxene analyses of sample D14, Table S13: pyroxene analyses of samples D2 and D6, Table S14: plagioclase literature data from the studied Marsili lavas.

Author Contributions: Conceptualization, T.T.; writing—original draft preparation, T.T. and M.P.M.; writing, review and editing, T.T. and M.P.M. All authors have read and agreed to the published version of the manuscript.

Funding: This research (sampling campaigns) was funded to M.P.M. by CNR under the Flagship Project RITMARE.

Institutional Review Board Statement: Not applicable.

Informed Consent Statement: Not applicable.

Data Availability Statement: The data presented in this study are all reported in Supplementary Materials: Text file, Figures S1–S7, Tables S1–S14.

Acknowledgments: We thank the anonymous reviewers for their constructive comments. We are very grateful to the scientists and crew onboard the sampling campaigns. We thank A. Comelli and D. Peis (University of Parma) for their help in the analytical work and R. Carampin (IGG-CNR, Padova Unit) for his assistance with the electron microprobe.

Conflicts of Interest: The authors declare no conflict of interest.

References

- Lee, A.; Bachmann, O. How important is the role of crystal fractionation in making intermediate magmas? Insights from Zr and P systematics. *Earth Planet. Sci. Lett.* **2014**, *393*, 266–274. [[CrossRef](#)]
- Martinez, F.; Taylor, B. Modes of crustal accretion in back-arc basins: Inferences from the Lau Basin. In *Back-Arc Spreading Systems: Geological, Biological, Chemical and Physical Interactions*, *Geophysical Monograph*; Christie, D.M., Fisher, C.R., Lee, S.-M., Givens, S., Eds.; American Geophysical Union: Washington, DC, USA, 2006; Volume 166, pp. 5–30. [[CrossRef](#)]
- Turner, S.J.; Langmuir, C.H. The global chemical systematics of arc front stratovolcanoes: Evaluating the role of crustal processes. *Earth Planet. Sci. Lett.* **2015**, *422*, 182–193. [[CrossRef](#)]
- Cashman, K.V.; Sparks, R.S.J.; Blundy, J.D. Vertically extensive and unstable magmatic systems: A unified view of igneous processes. *Science* **2017**, *355*, EAAG 3055. [[CrossRef](#)]
- Rudnick, R. Making continental crust. *Nature* **1995**, *378*, 571–578. [[CrossRef](#)]
- Grove, T.L.; Elkins-Tanton, L.T.; Parman, S.W.; Chatterjee, N.; Müntener, O.; Gaetani, G.A. Fractional crystallization and mantle-melting controls on calc-alkaline differentiation trends. *Contrib. Mineral. Petrol.* **2003**, *145*, 515–533. [[CrossRef](#)]
- Melekhova, E.; Annen, C.; Blundy, J. Compositional gaps in igneous rock suites controlled by magma system heat and water content. *Nat. Geosci.* **2013**, *6*, 385–390. [[CrossRef](#)]
- Melekhova, E.; Jon Blundy, J.; Robertson, R.; Humphreys, M.C.S. Experimental evidence for polybaric differentiation of primitive arc basalt beneath St. Vincent, Lesser Antilles. *J. Petrol.* **2015**, *56*, 161–192. [[CrossRef](#)]
- Nandedkar, H.R.; Ulmer, P.; Müntener, O. Fractional crystallization of primitive, hydrous arc magmas: An experimental study at 0.7 GPa. *Contrib. Mineral. Petrol.* **2014**, *167*, 1015. [[CrossRef](#)]
- Pichavant, M.; Macdonald, R. Crystallization of primitive basaltic magmas at crustal pressures and genesis of the calc-alkaline igneous suite: Experimental evidence from St Vincent, Lesser Antilles arc. *Contrib. Mineral. Petrol.* **2007**, *154*, 535–558. [[CrossRef](#)]
- Dahren, B.; Troll, R.V.; Andersson, B.U. Magma plumbing beneath Anak Krakatau volcano, Indonesia: Evidence for multiple magma storage regions. *Contrib. Mineral. Petrol.* **2012**, *163*, 631–651. [[CrossRef](#)]
- Geiger, H.; Troll, R.V.; Jolis, M.E.; Deegan, M.F.; Harris, C.; Hilton, R.D.; Freda, C. Multi-level magma plumbing at Agung and Batur volcanoes increases risk of hazardous eruptions. *Sci. Rep.* **2018**, *8*, 10547. [[CrossRef](#)]
- Jeffery, A.J.; Gertisser, R.; Troll, V.R.; Jolis, E.M.; Dahren, B.; Harris, C.; Tindle, A.G.; Preece, K.; O’Driscoll, B.; Humaida, H.; et al. The pre-eruptive magma plumbing system of the 2007–2008 dome-forming eruption of Kelut volcano, East Java, Indonesia. *Contrib. Mineral. Petrol.* **2013**, *166*, 275–308. [[CrossRef](#)]
- Kent, A.; Darr, C.; Koleszar, A.; Salisbury, J.M.; Cooper, M.K. Preferential eruption of andesitic magmas through recharge filtering. *Nat. Geosci.* **2010**, *3*, 631–636. [[CrossRef](#)]
- Ruprecht, P.; Plank, T. Feeding andesitic eruptions with a high-speed connection from the mantle. *Nature* **2013**, *500*, 68–72. [[CrossRef](#)] [[PubMed](#)]
- Cashman, V.K.; Edmonds, M. Mafic glass compositions: A record of magma storage conditions, mixing and ascent. *Phil. Trans. R. Soc. A* **2019**, *377*, 20180004. [[CrossRef](#)] [[PubMed](#)]
- Trua, T.; Marani, P.M.; Gamberi, F. Magmatic evidence for African mantle propagation into the southern Tyrrhenian back-arc region. In *Volcanism and Evolution of the African Lithosphere Special Paper*; Beccaluva, L., Bianchini, G., Wilson, M., Eds.; Geological Society of America: Boulder, CO, USA, 2011; Volume 478, pp. 307–331. [[CrossRef](#)]
- Trua, T.; Marani, M.P.; Gamberi, F. Magma plumbing system at a young back-arc spreading center: The Marsili Volcano, Southern Tyrrhenian Sea. *Geochem. Geophys. Geosyst.* **2018**, *19*, 43–59. [[CrossRef](#)]
- Di Stefano, F.; Mollo, S.; Ubide, T.; Petrone, C.M.; Caulfield, J.; Scarlato, P.; Nazzari, M.; Andronico, D.; Del Bello, E. Mush cannibalism and disruption recorded by clinopyroxene phenocrysts at Stromboli volcano: New insights from recent 2003–2017 activity. *Lithos* **2020**, *360–361*, 105440. [[CrossRef](#)]
- Maro, G.; Caffè, P.J.; Romer, R.L.; Trumbull, R.B. Neogene mafic magmatism in the northern Puna Plateau, Argentina: Generation and evolution of a back-arc volcanic suite. *J. Petrol.* **2017**, *58*, 1591–1617. [[CrossRef](#)]
- Preece, K.; Gertisser, R.; Barclay, J.; Berlo, K.; Herd, R.A. Pre- and syn-eruptive degassing and crystallisation processes of the 2010 and 2006 eruptions of Merapi volcano, Indonesia. *Contrib. Mineral. Petrol.* **2014**, *168*, 1061. [[CrossRef](#)]
- Trua, T.; Marani, M.P.; Barca, D. Lower crustal differentiation processes beneath a back-arc spreading ridge (Marsili seamount, Southern Tyrrhenian Sea). *Lithos* **2014**, *190–191*, 349–362. [[CrossRef](#)]
- Jackson, M.D.; Blundy, J.; Sparks, R.S.J. Chemical differentiation, cold storage and remobilization of magma in the Earth’s crust. *Nature* **2018**, *564*, 405–409. [[CrossRef](#)] [[PubMed](#)]
- Marani, M.P.; Trua, T. Thermal constriction and slab tearing at the origin of a superinflated spreading ridge: Marsili volcano (Tyrrhenian Sea). *J. Geophys. Res.* **2002**, *107*, 2188. [[CrossRef](#)]

25. Faccenna, C.; Becker, T.W.; Auer, L.; Billi, A.; Boschi, L.; Brun, J.P.; Capitanio, F.A.; Funiciello, F.; Horvath, F.; Jolivet, L.; et al. Mantle dynamics in the Mediterranean. *Rev. Geophys.* **2014**, *52*, 283–332. [[CrossRef](#)]
26. Kastens, K.A.; Mascle, J. The geological evolution of the Tyrrhenian Sea: An introduction to the scientific results of ODP Leg 107. *Proc. Ocean Drill. Program Sci. Results* **1990**, *107*, 3–26.
27. Tumanian, M.; Frezzotti, M.L.; Peccerillo, A.; Brandmayr, E.; Panza, G.F. Thermal structure of the shallow upper mantle beneath Italy and neighbouring areas: Magmatic activity and geodynamic significance. *Earth-Sci. Rev.* **2012**, *114*, 369–385. [[CrossRef](#)]
28. Putirka, K.D. Thermometers and barometers for volcanic systems. *Rev. Min. Geochem.* **2008**, *69*, 61–120. [[CrossRef](#)]
29. Mollo, S.; Del Gaudio, P.; Ventura, G.; Iezzi, G.; Scarlato, P. Dependence of clinopyroxene composition on cooling rate in basaltic magmas: Implications for thermobarometry. *Lithos* **2010**, *118*, 302–312. [[CrossRef](#)]
30. Ghiorsio, M.S.; Sack, R.O. Chemical mass-transfer in magmatic processes IV. A revised and internally consistent thermodynamic model for the interpolation and extrapolation of liquid-solid equilibria in magmatic systems at elevated-temperatures and pressures. *Contrib. Miner. Petrol.* **1995**, *119*, 197–212. [[CrossRef](#)]
31. Costa, F.; Morgan, D. Time constraints from chemical equilibration in magmatic crystals. In *Timescales of Magmatic Processes: From Core to Atmosphere*; Dosseto, A., Turner, S., Van-Orman, J., Eds.; Wiley: Chichester, UK, 2011; pp. 125–159. [[CrossRef](#)]
32. Stamper, C.C.; Blundy, J.D.; Arculus, R.J.; Melekhova, E. Petrology of plutonic xenoliths and volcanic rocks from Grenada, Lesser Antilles. *J. Petrol.* **2014**, *55*, 1353–1387. [[CrossRef](#)]
33. Langmuir, C.H.; Klein, E.M.; Plank, T. Petrological systematics of mid-ocean ridge basalts: Constraints on melt generation beneath ocean ridges. In *Mantle Flow and Melt Generation at Mid-Ocean Ridges*; Morgan, J.P., Blackman, D.K., Sinton, J.M., Eds.; Geophysical Monograph, American Geophysical Union: Washington, DC, USA, 1992; Volume 71, pp. 183–280. [[CrossRef](#)]
34. Muntener, O.; Kelemen, P.B.; Grove, T.L. The role of H₂O during crystallization of primitive arc magmas under uppermost mantle conditions and genesis of igneous pyroxenites: An experimental study. *Contrib. Mineral. Petrol.* **2001**, *141*, 643–658. [[CrossRef](#)]
35. Bouilhol, P.; Schmidt, M.W.; Burg, J.P. Magma transfer and evolution in channels within the arc crust: The pyroxenitic feeder pipes of Sapat (Kohistan, Pakistan). *J. Petrol.* **2015**, *56*, 1309–1342. [[CrossRef](#)]
36. Nakagawa, M.; Wada, K.; Wood, C.P. Mixed magmas, mush chambers and eruption triggers: Evidence from zoned clinopyroxene phenocrysts in andesitic scoria from the 1995 eruptions of Ruapehu volcano, New Zealand. *J. Petrol.* **2002**, *43*, 2279–2303. [[CrossRef](#)]
37. Petrone, C.M.; Braschi, E.; Francalanci, L.; Casalini, M.; Tommasini, S. Rapid mixing and short storage timescale in the magma dynamics of a steady-state volcano. *Earth Planet. Sci. Lett.* **2018**, *492*, 206–221. [[CrossRef](#)]
38. Stone, S.; Niu, Y. Origin of compositional trends in clinopyroxene of oceanic gabbros and gabbroic rocks: A case study using data from ODP Hole 735B. *J. Volcanol. Geoth. Res.* **2009**, *184*, 313–322. [[CrossRef](#)]
39. Ubide, T.; Kamber, B.S. Volcanic crystals as time capsules of eruption history. *Nat. Commun.* **2018**, *9*, 326. [[CrossRef](#)]
40. Cooper, G.F.; Davidson, J.P.; Blundy, J.D. Plutonic xenoliths from Martinique, Lesser Antilles: Evidence for open system processes and reactive melt flow in island arc crust. *Contrib. Mineral. Petrol.* **2016**, *171*, 87. [[CrossRef](#)] [[PubMed](#)]
41. Larocque, J.; Canil, D. The role of amphibole in the evolution of arc magmas and crust: The case from the Jurassic Bonanza arc section, Vancouver Island, Canada. *Contrib. Mineral. Petrol.* **2010**, *159*, 475–492. [[CrossRef](#)]
42. Neave, D.A.; Putirka, K.D. A new clinopyroxene-liquid barometer, and implications for magma storage pressures under Icelandic rift zones. *Am. Mineral.* **2017**, *102*, 777–794. [[CrossRef](#)]
43. Smith, D.J. Clinopyroxene precursors to amphibole sponge in arc crust. *Nat. Commun.* **2014**, *5*, 4329. [[CrossRef](#)]
44. Couch, S.; Sparks, R.S.; Carroll, M.R. Mineral disequilibrium in lavas explained by convective self-mixing in open magma chambers. *Nature* **2001**, *411*, 1037–1039. [[CrossRef](#)]
45. Dufek, J.; Bachmann, O. Quantum magmatism: Magmatic compositional gaps generated by melt-crystal dynamics. *Geology* **2011**, *38*, 687–690. [[CrossRef](#)]
46. Crabtree, S.M.; Lange, R.A. Complex phenocryst textures and zoning patterns in andesites and dacites: Evidence of degassing-induced rapid crystallization? *J. Petrol.* **2011**, *52*, 3–38. [[CrossRef](#)]
47. Streck, M.J. Mineral textures and zoning as evidence for open system processes. *Rev. Mineral. Geochem.* **2008**, *69*, 595–622. [[CrossRef](#)]